Accepted Manuscript

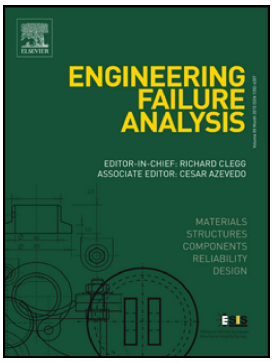

Longitudinal rail weld geometry control and assessment criteria

Ilaria Grossoni, Philip Shackleton, Yann Bezin, Jay Jaiswal

PII: S1350-6307(17)30468-5
DOI: doi: 10.1016/j.engfailanal.2017.07.008
Reference: EFA 3226

To appear in: *Engineering Failure Analysis*

Received date: 10 April 2017
Revised date: 23 June 2017
Accepted date: 5 July 2017

Please cite this article as: Ilaria Grossoni, Philip Shackleton, Yann Bezin, Jay Jaiswal , Longitudinal rail weld geometry control and assessment criteria, *Engineering Failure Analysis* (2017), doi: 10.1016/j.engfailanal.2017.07.008

Longitudinal rail weld geometry control and assessment criteria[1]

Ilaria Grossoni[2], Philip Shackleton, Yann Bezin, Jay Jaiswal

Institute of Railway Research, University of Huddersfield, Huddersfield, UK

This study covers the parametric variations of vehicle and track characteristics to inform on the requirements for an optimum and yet pragmatic control of longitudinal rail weld profile. A statistical study has been carried out using a large set of measured weld profiles (arbitrary mix of flash butt welds and aluminothermic welds) in order to establish relationships between degradation mechanisms and the longitudinal geometry of the finished weld. The potential benefits which would be expected from improved controls over the welded profile, with respect to not only rail running surface damage but also susceptibility to rail breaks and ballast degradation, are demonstrated. Finally, recommendations for the review of the geometric controls of finished weld geometry in the relevant Euro Norms are made.

Keywords: Geometry assessment; longitudinal weld profile; rail fatigue; vehicle/track interaction; wheel/rail contact forces.

1. Introduction

There is a continuing worldwide trend towards installing continuously welded rails (CWR) to minimize the wheel-rail impact forces in comparison to jointed track. Even though the use of welding to join rails is a considerable

---

[1]

BOEF	Beam on Elastic Foundation
CWR	Continuously Welded Rails
FE	Finite Element
HAZ	Heat Affected Zones
RCF	Rolling Contact Fatigue
SFT	Stress Free Temperature
UTS	Ultimate Tensile Stress
VTI	Vehicle/Track Interaction

[2] Corresponding author: Ilaria Grossoni, Institute of Railway Research, University of Huddersfield, Queensgate, HD1 3DH Huddersfield (UK), i.grossoni@hud.ac.uk, Tel: +44 (0)1484 471179

improvement, all existing rail welding processes require finish grinding, which may introduce a localised short-wave irregularity, usually over one metre or less. This finishing process, particularly in the case of manual profile grinding, does not guarantee a crown profile as smooth as a hot rolled rail. This imperfect geometry may, in some cases, lead to high dynamic contact forces, contact stresses and sub-surface shear stresses. These in turn drive damage mechanisms such as cupping (i.e. localised plastic deformation associated with material non-homogeneities along the wheel and rail surface – see the second bullet point), squat defects, corrugation, and other induced degradation mechanisms, such as differential settlement of ballast around the weld, uneven sleepers and, potentially, increased rail bending stress. It has been shown in Ishida [1] that general looseness of sleepers around the weld area causes a significant reduction of the rail fatigue life. The damage is due to two main reasons [2]:

- Geometric irregularity at the wheel/rail interface, causing dynamic vertical load variations, and increased contact stresses on the rail following the weld;
- Material non-homogeneities along the wheel and rail surface. In particular, there are zones near the weld, the so-called heat affected zones (HAZ), which are characterised by different properties and microstructure compared to that of the parent rails, leading to a very noticeable variation in hardness and resistance to wear and plastic deformation. Furthermore, in the case of aluminothermic welds, the relationship between hardness and the resistance to wear is also influenced by the different microstructure properties of the weld metal (i.e. cast microstructure in the weld material and rolled microstructure for the parent rail). Thus, the wheel contacts the parent rail microstructure, then that in the heat affected zone followed by that in the weld metal. The deterioration of profile in service in these three regions is a function of the material properties.

This study, which is part of the European Project WRIST [3], is mainly focussed on the first of these two reasons.

The existing Euro Norms (such as that for aluminothermic welds [4] and for flash butt welds [5]) employ simplistic metrics to assess the quality of the finished weld geometry. This is a zero-derivative based method which only considers the maximum peak value along the welding zone. These metrics do not reflect the significant advances in metrology and the understanding of rail damage, which have been made in recent years. The Dutch infrastructure manager ProRail [6] has adopted a more sophisticated standard that employs a metric which requires a (comparatively) detailed longitudinal measurement of the rail running surface. This is a first-derivative based method which considers the maximum of the first derivative of the weld profile over one metre (hereafter, referred as “maximum absolute gradient”). The limits imposed in the Dutch standard are derived from the relationship between rail geometry (absolute gradient), wheel-rail interaction forces and vehicle speed [7-10]. In the context of high speed lines, a recent study by

Gao [11] recommends a control of both wavelength and amplitude of rail weld irregularity in order to limit the wheel-rail dynamic response.

Regarding the support degradation, in Mutton [12] it has been shown that poor support under welds contributes to increase the dynamic load impact factor by up to 50% for a given maximum irregularity over one metre. In Ishida [1], the influence of unsupported sleepers on the predicted fatigue life has been assessed and it has been demonstrated that the presence of 2 hanging sleepers with 2 mm gap reduces the fatigue life to approximately half that for the case of fully supported sleepers. Therefore, it is essential to take into account the general uneven support around the weld area during the dynamic analysis of the wheel/rail interaction.

The aim of this study is to build on the existing work of Steenbergen [7-10], which led to the creation and justification for the Dutch standard, through wider independent parametric studies. The scope of investigation is extended to include a greater range of input parameters, including track parameters (i.e. support stiffness, sleeper type and spacing, rail type) and vehicle parameters (i.e. USM and primary suspension characteristics), and to consider a broad range of rail and track damage metrics, including bending stresses, rail-pad forces and ballast forces.

In Section 2 the vertical vehicle/track interaction model used to predict these damages is established. The parametric study using both theoretical (Section 3.1) and measured (Section 3.2) weld profiles is presented and the main conclusions are summarised in Section 3.3. Revised control measures based on considerations of rail bending stresses and rail fatigue life are demonstrated in Section 4. Finally, recommendations for the review of the geometric controls of finished weld geometry in the relevant Euro Norms are made in Section 5.

2. Vertical vehicle/track interaction model

The vertical vehicle/track interaction (VTI) model used for the parametric studies is shown in Figure 1 (Grossoni [13]).

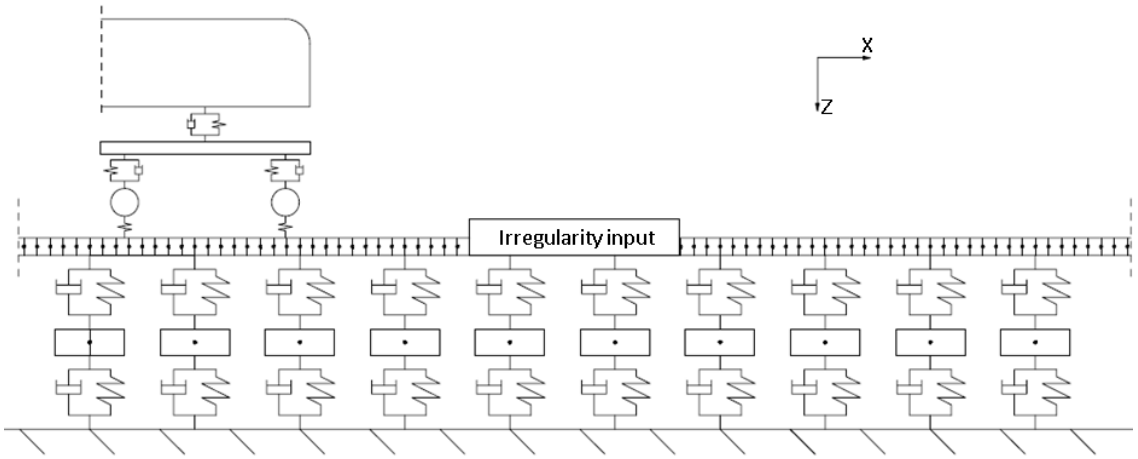

Figure 1: Vertical VTI model with an arbitrary irregularity (x-z plane).

The track consists of two-layer discretely supported ballasted track, accounting for the rails shear and bending modes, the sleeper's vertical movement and the rail-pads and ballast resiliencies. The rail is modelled based on Timoshenko beam theory and a finite element (FE) approach is developed so that the deformation within each rail element is approximated using nodal values of displacements and rotations. A total length of 24 metres has been considered for this study to ensure numeric stability is achieved before the 1 m irregularity of interest. This also ensures no boundary effects and the first and the last rail nodes are considered pinned.

The vehicle model consists of half the car body, one bogie and two wheelsets connected with primary and secondary suspensions. All the bodies are assumed to be rigid and all the masses are concentrated at the centre of gravity of the corresponding element.

Assuming a single point of contact at each wheel, the non-linear Hertzian contact model is used to couple the vehicle and track models. According to this law, the contact force is derived as:

$$P_z = \begin{cases} K_H(\delta_{wr})^{3/2} & \text{if } \delta_{wr} \geq 0 \\ 0 & \text{if } \delta_{wr} < 0 \end{cases} \quad (1)$$

Where:

P_z = vertical wheel/rail contact force [N];

δ_{wr} = vertical wheel/rail penetration (wheel lift if negative) [m];

K_H = Hertzian contact parameter [$N/m^{3/2}$].

The vertical wheel/rail penetration δ_{wr} (considered positive downwards) is calculated with the relative displacement between wheel and rail including the irregularity profile due to the weld. Initially the model was successfully compared and matched against available literature (Steenbergen [8]). The validation of the model against experimental observations is out of the scope of this paper, and will be considered in future work.

In a first stage the longitudinal weld profile has been modelled with a theoretical profile as a sinusoidal wave over 1 metre with a maximum height W and a triangular wave over length L with a maximum height V above the sinusoidal wave (Figure 2). This idealised case is to take into account the elementary possibilities in the surface of real weld [8]. This has been done to assess the most influential parameters.

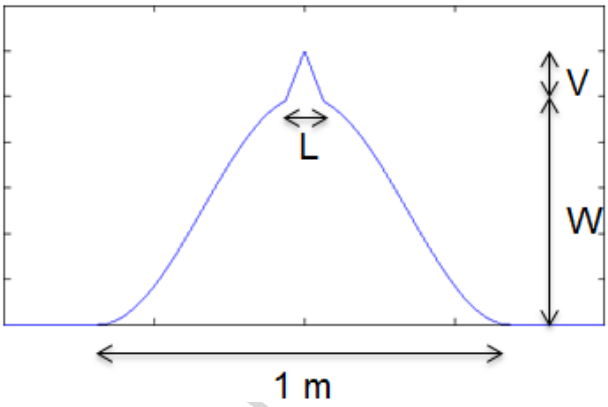

Figure 2: Example of theoretical longitudinal weld profile.

In a second stage, 110 measured weld profiles (an arbitrary mixture of flash butt welds and aluminothermic welds) have been considered. The measurements have been undertaken with the RAILPROF device ([14]) on a rail network under a regime with geometric controls as per the applicable Euro Norms [4, 5] (manual assessment with a steel straightedge and a feeler gauge). Even though such a regime no longer applies there, the welds are expected to be representative for those networks still using the methodology described in the reference EN norm. Note that this is a sub-set of the data used in Steenbergen [8] shared within the WRIST consortium.

The outputs of the model considered in this study are the following:

- P1 and P2 impact forces (Jenkins [15], Figure 3): to assess the damage at the rail level (P1 force) and at the ballast level (P2 force). Only the dynamic component is quoted hereafter;
- Rail-pad forces: to assess the possible damage to the fixing system;
- Bending stresses: to assess the propensity for fatigue failure due to cracks in the rail foot;

- Ballast degradation: in this study the ballast force is used as an assessment index. Even if the P2 force gives an idea of ballast damage, the information about the position is lost, as the peak value can occur in different locations depending on a variety of factors (e.g. travelling speed, support stiffness, sleeper spacing, rail second moment of area). Therefore, it is worth having an additional parameter that takes directly into account the position.

In particular, the P1 forces are calculated as the maximum of the unfiltered wheel/rail contact forces and the P2 forces as the maximum of the filtered wheel/rail contact forces below 200 Hz. This value has been chosen to take into account all the parametric variations that have been carried out.

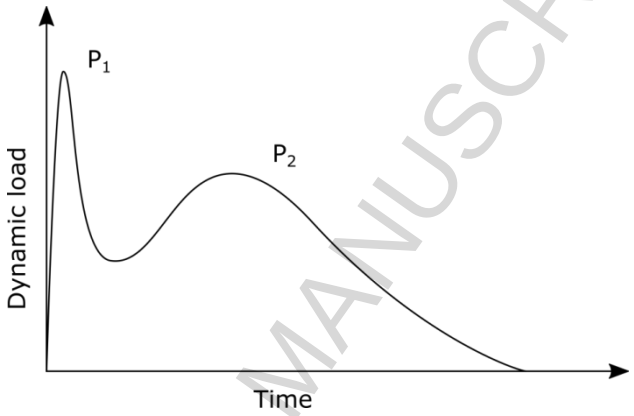

Figure 3: P1 and P2 impact forces at an interface irregularity on ballasted track [7].

3. Parametric studies

3.1. Parametric study with theoretical profiles

In this study, the parameters and values tabulated in Table 1 and Table 2 are considered. The motivation for each parameter choice is explained in detail in the corresponding row.

Table 1: Parametric variations considered in the present study.

	Parameter	Values	Motivation
Speed	Speed [km/h]	40/80/**140**/200/300	Speed categories in the Dutch standard [6]
USM	Unsprung mass (half) [kg]	400/**800**/1200/1500	To represent freight/passenger vehicles
Kp	Primary suspension stiffness [MN/m]	0.2/0.5/**1**/2	To represent passenger/freight vehicles
Kb	Support stiffness [MN/m/sleeper end]	12/**24**/61	As in Eurobalt project [16], to represent poor (40 MN/m), medium (80 MN/m) and hard (200 MN/m). Includes a correction factor of 0.3 to take into account the generally poorer support condition around the weld
l	Sleeper spacing [m]	0.5/**0.6**/0.7/0.8	50E1/54E1/55E1/60E1 ([17])
Izz	Rail second moment of area [cm^4]	1987/**2338**/2150/3038	
m	Rail mass [kg/m]	50.4/**54.8**/56.0/60.1	
W	Geometrical variation	As in Table 2	Cases considered in Ishida [1]
gap	Gap of 2 hanging sleepers [mm]	**0**/3/5	
ms	Sleeper mass (half) [kg]	50/100/**150**	Timber/twin block/concrete sleepers [18]

Table 2: Weld geometrical variation (the parameters are in relation to Figure 2) [1].

Parameter [mm]	Values						
	Case 1	Case 2	Case 3	Case 4	Case 5	Case 6	Case 7
W	**1**	1	1	1	0.6	0.4	0.8
V	**0.2**	0.2	0.2	0.8	0.6	0.1	0.1
L	**100**	50	200	100	100	250	250

The effect of each parameter has been explored independently considering all the others as nominal (bold values in Table 1 and Table 2).

Six additional cases are also considered to represent a number of cases with parameter combinations as shown in Table 3.

Table 3: Parameter values for combined cases.

Parameter	1	2	3	4	5	6
Vehicle type	*Freight*	*Freight*	*Freight*	*Passenger*	*Passenger*	*Passenger*
Ballast layer type	*Weak*	*Medium*	*Good*	*Weak*	*Medium*	*Good*
Speed [km/h]	80	80	80	200	200	200
USM (half) [kg]	800	800	800	1500	1500	1500
Primary suspension stiffness [MN/m]	2	2	2	0.5	0.5	0.5
Support stiffness [MN/m/sleeper end]	12	24	61	12	24	61
Sleeper spacing [m]	0.8	0.7	0.6	0.8	0.7	0.6
Rail second moment of area [cm^4]	1987	2150	3038	1987	2150	3038
Rail mass [kg/m]	50.4	56.0	60.1	50.4	56.0	60.1
Sleeper mass [kg]	150	150	150	150	150	150

In the first instance, the most influential parameters for the range of variation of P1 force and bending stresses on the rail foot are summarised in Table 4. These two outputs have been chosen as they are the most important for the rest of

the work representing the damage at the rail level (see Dutch standard [6]) and a proxy of the weld fatigue life (see Section 4). The increases of highest values with respect to lowest which are greater than 15% are highlighted in red. This threshold has been chosen as 3 times the margin of error tolerance (considered at 5%).

Table 4: Range of variation of P1 force and bending stresses on the rail foot.

	Minimum P1 [kN]	**Maximum P1 [kN]**	**Difference**	**Minimum stress [MPa]**	**Maximum stress [MPa]**	**Difference**
Speed	82.3	129.9	57.8%	117	154.4	32.0%
USM	104.3	122.2	17.2%	110.2	131.7	19.5%
Kp	105.2	113.5	7.9%	131.7	134.8	2.4%
Kb	109	127.3	16.8%	122.4	141.1	15.3%
gap	143.2	172.3	20.3%	123.6	165.8	34.1%
l	102.8	114.3	11.2%	110.3	140.1	27.0%
Izz	110.7	112.4	1.5%	108	148.7	37.7%
m	110.8	111.9	1.0%	131.6	132.2	0.5%
ms	108.8	116.3	6.9%	126.3	136.7	8.2%
W	106.3	237.9	123.8%	125.4	155.8	24.2%
Combined cases (Table 3)	128.6	192	49.3%	103.1	179.2	73.8%

Table 4 shows that the most influential parameters in both criteria analysed are speed, USM, support stiffness, hanging sleepers and extreme cases, in addition to the weld geometrical variation.

In Figure 4 an example of the effect of speed on P1 force, P2 force, ballast forces and rail bending stresses for increasing maximum absolute gradient is presented.

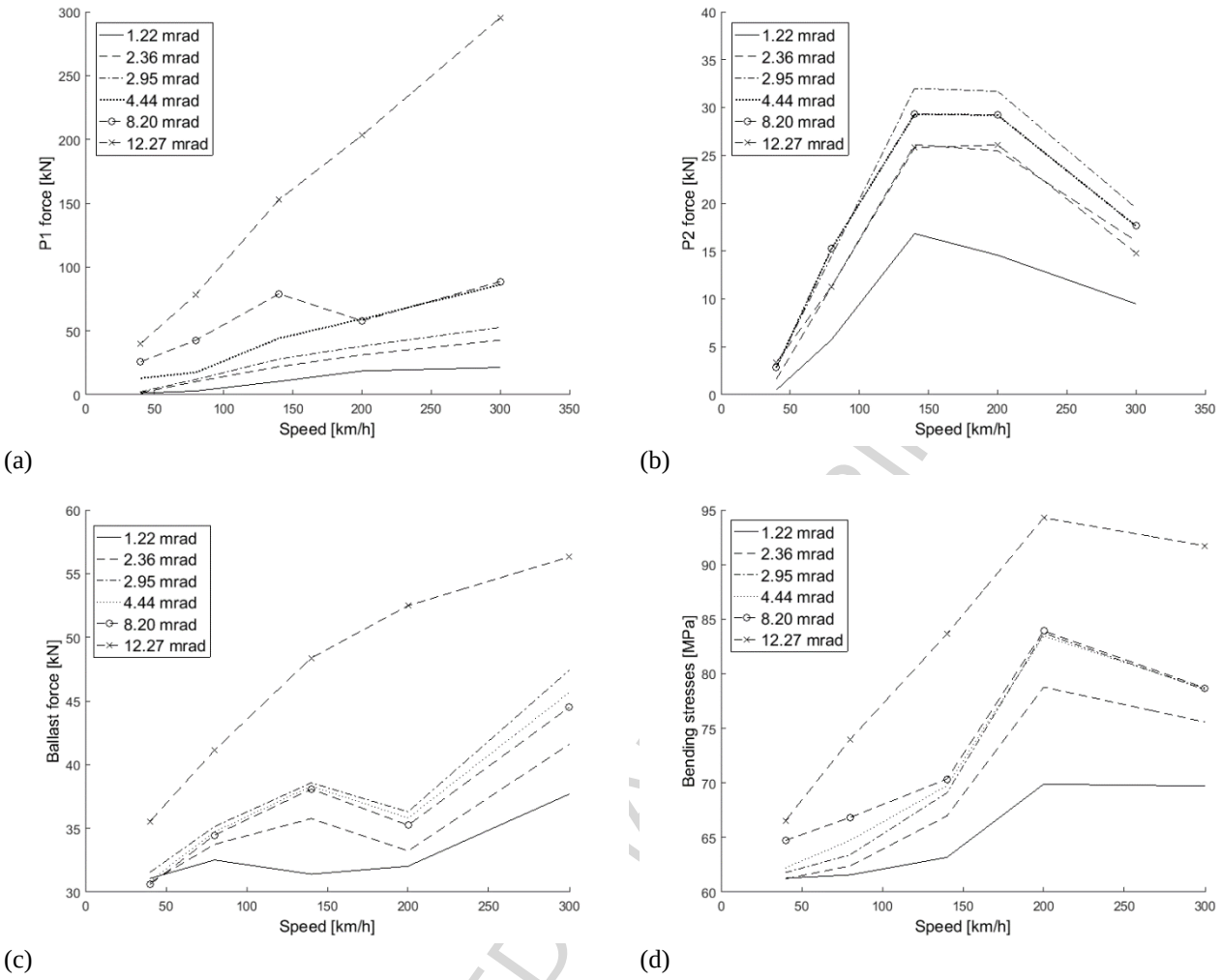

Figure 4: The influence of speed on (a) P1 force, (b) P2 force, (c) ballast forces and (d) rail bending stresses varying the irregularity geometry.

Figure 4a shows a trend of linear increase of P1 force (main contribution to rail surface and subsurface damage mechanisms) with increasing speed and with progressively worse geometry. In particular, the P1 force increases from 2.28 kN to 21.31 kN (834%) with increasing speed in case of the smoothest weld geometry and from 40 kN to 295 kN (637%) in case of the worst one. This means that increasing the line speed requires a better geometry for a given traffic type and, thus, more restrictive requirements. This is in line with previous works and the current Dutch standards [6]. In some extent, also the Euro Norm allows a relaxation of the allowable tolerances in case of lines with lower speed ([4, 5]).

On the contrary, the P2 force (main contribution to ballast damage mechanisms) increases with increasing speed and with progressively worse geometry in case of low to medium speed up to 140 km/h and then decreases for higher speeds (Figure 4b). In the latter case the wheel tends to fly over the irregularity instead of following it and the impact

occurs later and with lower magnitude.

Similarly to the contact forces, in the case of ballast forces the line speed plays a critical role, as shown in Figure 4c. There is an increase in force levels in the ballast layer for increasing speed or decreasing weld quality, with an average increment of ca. 21% in case of good weld geometry and ca. 59% in case of poor weld geometry. These increments are moderate in comparison with those observed for the P1 force and force in the rail-pads. This is because the rail-pads filter out the higher frequency content of the contact forces, thus reducing the peak values.

From Figure 4d, it is possible to notice an exponential increase of bending stresses with speeds up to 200 km/h and with increasing maximum vertical irregularity gradient. The average increase is ca. 15% in the case of good quality geometries and 40% in the case of bad quality geometries. This finding is broadly in line with those in Figure 4(b), as expected the P2 force tends to drive overall track deflection and therefore rail bending.

Table 5 summarises the main findings for the parametric study with theoretical weld profiles.

Table 5: Summary of findings (▲▲: change >50% with varying geometry; ▲: change >20% and <50% with varying geometry; -: change<20% with varying geometry).

Parameter	**P1 force**	**P2 force**	**Rail-pad force**	**Ballast forces**	**Bending stresses**
Increasing speed	▲▲	▲	▲▲	▲	▲
Increasing USM	▲	▲	▲	▲	▲
Increasing support stiffness	▲	▲▲	▲	▲▲	▲
Extreme cases (low speed/high axle load)	▲	-	-	▲	▲
Extreme cases (high speed/low axle load)	-	▲▲	▲▲	▲▲	▲

The results from Table 5 show that in the cases of theoretical profiles considered:

- Increasing speed requires better weld geometry to limit, principally, the P1 force and the rail-pad force;
- Increasing USM has a moderate effect on all quantities considered;
- A better weld geometry would be preferred with a higher support stiffness track, to lower or minimise the magnitude of P2 and ballast forces;
- In the case of low speed and high axle load, changing the support conditions has a moderate effect on the ballast forces and the bending stresses;

- In case of high speed and low axle load, changing the support conditions has a very significant effect on P2 force, rail-pad forces and ballast forces and a moderate influence on bending stresses.

In conclusion, good weld geometry (i.e. low maximum absolute gradient) is strongly reccomended in

- high speed lines,
- low quality support with voids,
- good quality and high stiffness track,
- low speed lines and high tonnage.

The thresholds considered depend on the actual maximum dynamic admissible forces.

3.2. Parametric study with measured profiles

The parameters and values reported in Table 6 are considered in the following calculations.

Table 6: Parametric variations considered in the present study.

Parameter	Values	Motivation
Speed [km/h]	40/80/**140**/200/300	Speed categories in [6]
USM (half) [kg]	400/**800**/1200/1500	Freight/passenger vehicles
Support stiffness [MN/m]	15/20/**30**/40/60/80	Values reflecting the correction factor as specified in Table 1

The effect of each parameter has been explored considering all the others as nominal (in bold). The other parameters are as in Table 1.

In these simulations the measured weld profile/irregularity was smoothed with a moving average filter over 5 points (25 mm) to remove the roughness component in the order of less than the dimension of a typical contact patch, which are practically ineffective in exciting the wheel and the rail [7, 19]. Apart from the methods based on the maximum allowable vertical alignment, there are two main approaches in the literature to assess the vertical weld profile [7]:

- First derivative-based methods: these are sensitive to irregularity with a global scale of 0.5 m;
- Second derivative-based methods: these are sensitive to irregularity with a global scale of some centimetres.

Since the weld is a localised irregularity over one metre, all the following graphs refer to the dynamic component of

forces and stresses against the maximum absolute gradient (i.e. maximum first derivative of the weld profile).

In Figure 5 the variation of the dynamic component of P1 force, P2 force, ballast force and rail bending stresses against the maximum absolute gradient for increasing speed is presented. Each point corresponds to a weld and the colour code corresponds to the line speed. For each speed considered, a regression line is plotted and the coefficient of determination (R^2) and the standard deviation (RMSE) are reported. The coefficient of determination is defined as the square root of the correlation between the predicted and the observed values, while the standard deviation as the root mean square error associated with each of the line. Note that data is considered slightly dispersed when R^2 is higher than 0.7, moderately dispersed when R^2 is between 0.3 and 0.7, highly dispersed when R^2 is lower than 0.3. The scatter in the data is explained with the fact that different weld profiles with the same maximum absolute gradient can give different output force value.

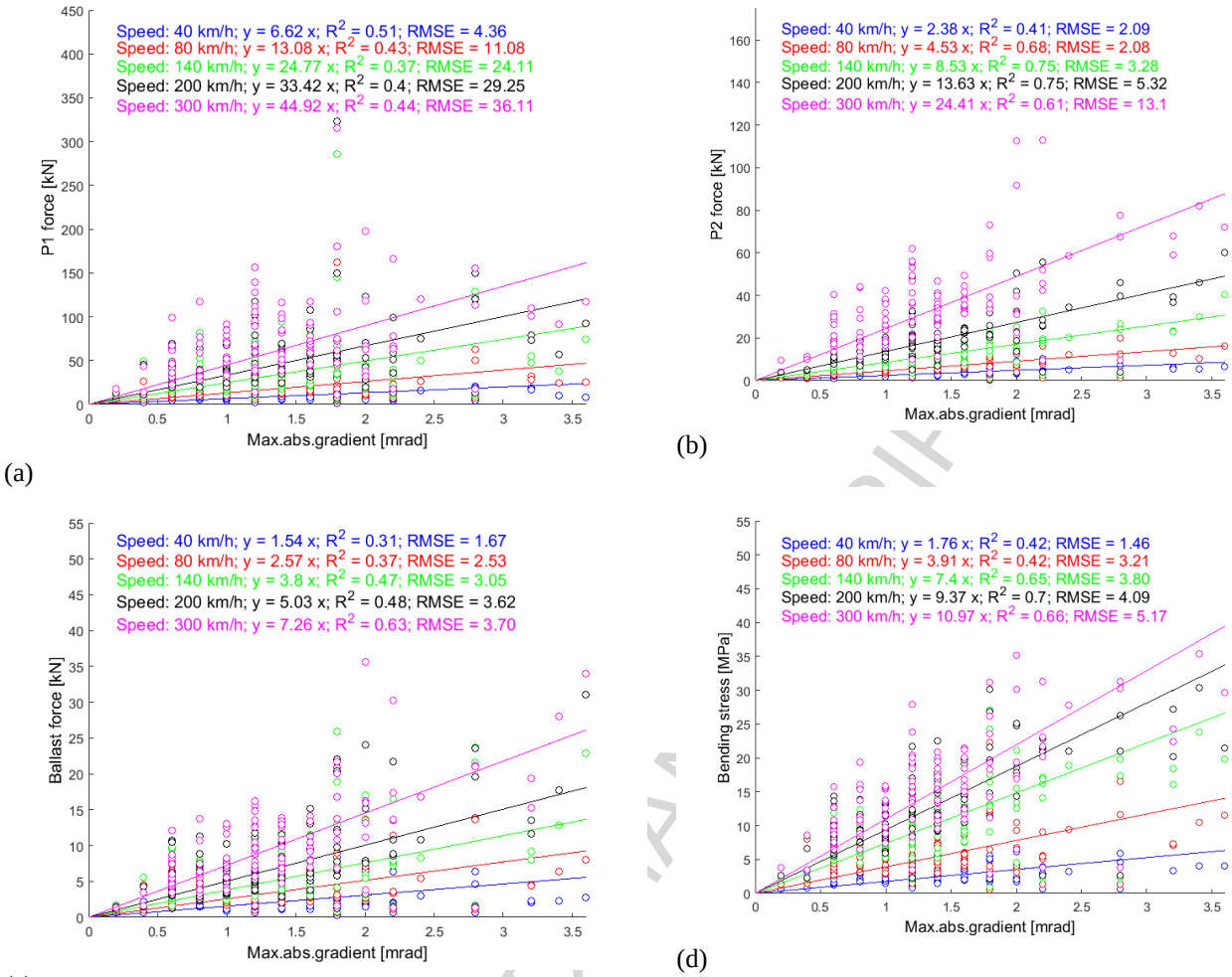

Figure 5: The influence of speed on the dynamic component of (a) P1 force, (b) P2 force, (c) ballast forces and (d) rail bending stresses (R^2: R-squared value of the regression line per each line speed considered; RMSE: standard deviation per each line speed considered).

Table 7 summarises the R^2 values for each case considered in Figure 5.

Table 7: R^2 values for P1 force, P2 force, ballast forces and rail bending stresses varying with speed.

Speed	P1 force	P2 force	Ballast forces	Rail stresses
40	0.51	0.41	0.31	0.42
80	0.43	0.68	0.37	0.42
140	0.37	0.75	0.47	0.65
200	0.40	0.75	0.48	0.70
300	0.44	0.61	0.63	0.66

Figure 5a shows that there is an increase of the dynamic component of P1 force with decreasing weld quality and with increasing speed. The influence of the speed is outlined by the rise of the regression line slope. Therefore, at higher speeds a better geometry is required to achieve the same dynamic force as at lower speed. This is in line with the work

in Steenbergen [8, 20]. Regarding the dispersion, it remains similar across all speeds.

As in the previous case, the dynamic component of the P2 force is strongly affected by the weld geometry and there is an increase of P2 force with increasing speed (Figure 5b). There is an increment of regression line slope of ca. 10 times from the lowest speed (i.e. 40 km/h) to the high speed (i.e. 300 km/h), demonstrating that the influence of geometry on P2 force increasingly important with increasing speed. Moreover, the coefficient of determination is reasonably high for all the speed cases considered. This suggests that there is a strong relationship between P2 force and weld geometry gradient. This will be explored in the following Sections.

Figure 5c shows that the dynamic component of ballast forces is strongly affected by the geometry and by increasing speed. In particular, there is an increment of regression line slope of ca. 7 times from the lowest speed (i.e. 40 km/h) to the highest speed (i.e. 300 km/h), similarly to the dynamic component of P2 force. Moreover, the coefficient of determination increases for increasing speed, going from a low correlation in case of low speeds (i.e. 40/80 km/h) to a good correlation in case of the highest speed (i.e. 200/300 km/h).

From Figure 5d it is possible to conclude that the dynamic component of rail bending stresses is largely affected by the weld geometry and the travelling speed. Increasing the weld gradient there is an increase in the bending stresses, with the increment considerably rising with increasing speed.

Table 8 summarises the main findings of this Section.

Table 8: Summary of findings (the considered output is *highly/moderately/slightly* affected by the weld geometry and the parameter - 3/2/1 markers respectively; the considered output is *highly/moderately/slightly* dispersed - ▲/■/● markers respectively).

Parameter	Speed	USM	Kb
P1 force	■■■	■	■
P2 force	■■■-▲▲▲	▲▲	▲▲
Rail-pad force	●●	●	●●
Rail bending stresses	■■■	■■■	■■-▲▲
Ballast forces	■■	■	■■■

The results from Table 8 show that:

- Improved weld geometry is required for higher speed track to minimise the P1 and P2 forces and the rail bending stresses;
- Increasing USM requires a better weld geometry to limit P2 force and rail bending stresses;

- for high quality support track, a better weld geometry is required to limit, principally, the P2 force and the ballast force. However, worse geometries are acceptable when bending stresses are considered.

To conclude, good weld geometry (i.e. low maximum absolute gradient) is strongly required in high speed lines, low quality support and high axle load.

3.3. Main conclusions from the parametric study with theoretical and measured profiles

From the parametric study with theoretical and measured weld profiles it was concluded that:

- Development of high speed routes requires a change in the weld geometry standards;
- The risk of reduced rail fatigue life and propagation of defects is lowered with improved weld geometry for track with lower quality support;
- Current levels of weld geometries are less tolerant of poor support stiffness created by voids;
- Increasing axle load or the number of axle passes is detrimental for the weld geometry.

The quantities mostly affected are:

- contact forces, which may be used as an indicator of rail surface damage, including wear and rolling contact fatigue (RCF);
- rail bending stresses, which are a measure of rail fatigue;
- ballast force, which are a measure of ballast degradation and differential settlement.

Note that the simultaneous variation of track and vehicle parameters has not been explored for the case of measured welds and, thus, it is not possible to draw any conclusion for that case.

From the main conclusions of the parametric study it is possible to deduce that it is fundamental to look at additional quantities to the wheel/rail contact forces in order to protect the whole system. The following section presents discussions taking into account the rail bending stresses as a measure of the rail fatigue life.

4. Revised controls based on rail bending stresses

The failure mode addressed in this Section is foot failures at the edge of the sleeper, where there is a high stress concentration from the rail bending imposed by the wheel passage. Although there is an increase in propensity for a

break due to surface cracking and crack growth within the HAZ[3], it was decided to concentrate here on where maximum rail stresses were predicted near the edge of the sleeper, where rail breaks are known to occur. Note that the fatigue failure within the weld, which is influenced by several factors including the presence of the weld collar, possible centreline shrinkage, defects in the foot, lack of fusion, porosity, elevated residual stress levels, etc. [21] is not considered. Also, the effect of the position of the weld with respect to the sleepers has not been addressed in the current study. These remain areas for further work.

According to Whitney [22], the rail breaks at welds in UK decreased by 10% between 2010-11 and 2014-2015, the head defects decreased by 2%, while the rail breaks at rail foot increased by 16% (Figure 6) which further supports the chosen failure mode of focus here.

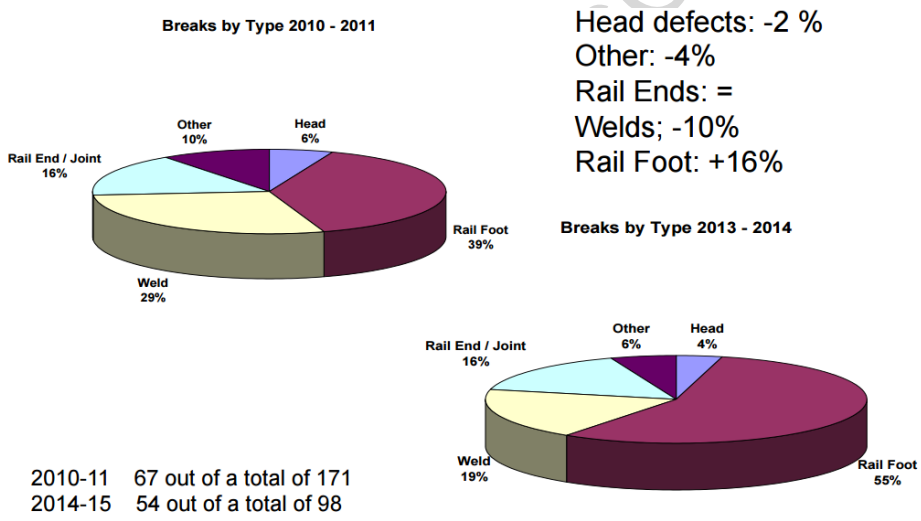

Figure 6: Distribution of rail breaks between 2010-2011 and 2014-2015 ([22]).

The rail bending stresses influence rail fatigue life when combined with the residual stresses in the rail from manufacturing and the stresses imposed during track laying. If the combined stresses are lower than the fatigue stress limit, the rail is not expected to fail through high cycle fatigue, except in the presence of stress concentration due to defects such as corrosion pits. If the rail bending stresses are higher than the limit, instead, fatigue damage will accumulate at each stress cycle, eventually leading to high cycle failure. With greater exceedance of the fatigue stress limit, the rail fatigue life shortens and degradation mechanisms, such as crack initiation, propagation and eventual

[3] Note that the transversal weld geometry is needed if the RCF within the welding area is studied.

fracture, are more likely to occur [23].

Non-uniformity of material properties along the running band of wheel/rail contact is a key factor that exacerbates the imperfect weld geometry inherited from manufacturing and installation. In particular, the HAZ is characterised by different mechanical properties and microstructure compared to that of the parent rails, leading to a noticeable variation in hardness [2] and wear resistance [24] that results in further deterioration of the geometry. Measured hardness data shows that the maximum variation occurs within 50-100 mm from the centre of the weld, while the maximum bending stresses occur well outside the HAZ (Figure 7). Therefore, the ultimate tensile stress (UTS) of the parent rail steel will be considered for the following calculations.

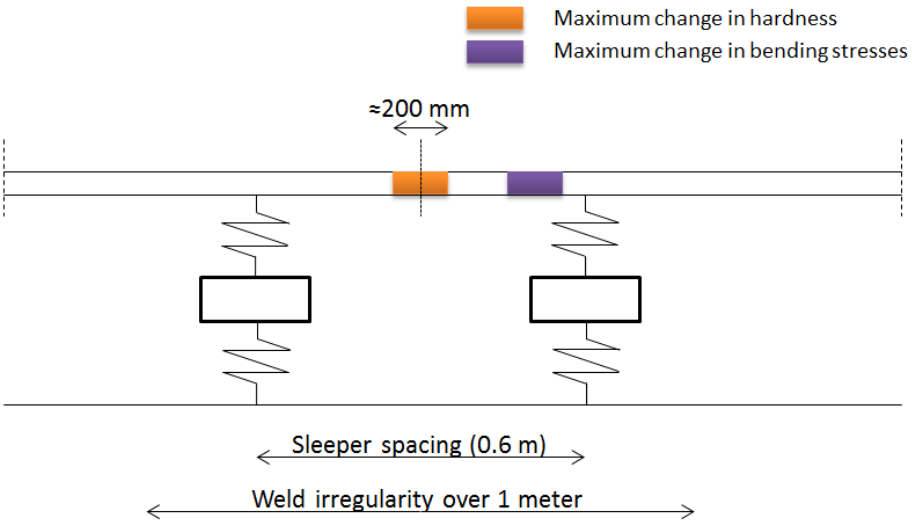

Figure 7: Area of maximum change in hardness and maximum change in bending stresses.

According to Murray [23], the fatigue stress limit can be approximated from to the ultimate tensile strength (UTS) as:

$$\sigma_{f,max} = 0.4 \cdot UTS \quad (1)$$

Where:

$\sigma_{f,max}$ = fatigue stress limit [MPa];

UTS = ultimate tensile strength [MPa].

Since the fatigue limit is affected by the surface finish, the approximation in (1) is valid for a certain 'reasonable' surface roughness. For the case of poor surface finish or high roughness, such as corrosion pitting (as can occur between

the rail and pad) or from poor quality manual finishing, this approximation will overestimate the fatigue stress limit. The controls subsequently developed here are therefore only strictly valid for an assumed nominal surface finish; however it will be seen that the theory could easily be applied to a different surface roughness by revising the applied fatigue stress limit.

Considering three steel grades analysed in the WRIST project [17], Table 9 shows the UTS, the fatigue stress limit of the material, the residual stress according to European Standard [25] (taken for the worst case of the maximum permissible remaining stress) and the remaining fatigue threshold, which represents the fatigue stress limit less the maximum permissible remaining stress. Note that, although the European Standard does not differentiate between these grades in the context of the residual stresses in the foot, the reality is that, to achieve the straightness mandated in the specifications, the higher yield strength materials need greater loads and hence develop higher residual stresses.

Table 9: Calculated fatigue stress capacity for three rail steel grades (all values in MPa).

Steel grade	**UTS**[4]	**Fatigue stress limit ($\sigma_{f,max}$)**	**Residual stress (σ_{res})**	**Remaining fatigue threshold ($\sigma_{f,max} - \sigma_{res}$)**
R260	880	352	250	102
R350HT	1175	470	250	220
R400HT	1280	512	250	262

The net imposed stress on the rail foot is the sum of the installation stress and thermal stress $\sigma_{\Delta T}$, which have been considered together, static stress σ_s and the dynamic bending stress from vehicle passages σ_d. It should be not higher than the remaining fatigue threshold $\sigma_{f,max} - \sigma_{res}$ to avoid fatigue failure:

$$\sigma_s + \sigma_d \leq \sigma_r - \sigma_{\Delta T} = \sigma_{f,max} - \sigma_{res} - \sigma_{\Delta T} \quad (2)$$

The static component is mainly influenced by the nominal wheel load and how it is distributed by the rail section, sleeper spacing, track stiffness (i.e. rail-pad and support stiffness). The dynamic component is influenced by the track geometry, the support stiffness, the unsprung mass and the vehicle speed. The installation stress is set as a function of the stress free temperature (SFT) and thermal stress vary according to the change from the SFT. Finally, the remaining

[4] These values are for a position in the rail head. In case of grade R260, the strength of head and foot are very similar as they are both air-cooled. In case of R350HT, the strength in the rail foot depends on the heat treatment methodology and, thus, may be slightly lower than the head. This is also applied to R400HT. However, the principles demonstrated in the calculations remain valid.

fatigue threshold depends on the steel grade.

Consequently, the total stress at the rail foot at the imposed limit of each speed category has been calculated as the sum of bending stress due to the static load, the additional dynamic stress taken from the regression lines (Figure 5) and thermal stresses ([26]). It is worth noting that in this process the variability around the mean value of the dynamic component is taken into account, by considering the regression line plus 2 times the standard deviation RSME. In this way 95% of data set is represented by the values used. In Table 10 and Figure 8 the total stress is compared with the remaining stress capacity depending on the variation from the SFT and the steel grade (Table 9). The cells highlighted in red are the cases in which the stress at the imposed limit exceeds the remaining fatigue threshold.

Table 10: Comparison between the stress at the imposed limit and the remaining fatigue threshold for each speed category considering three rail steel grades and three variations from the SFT (54E1 rail profile, 30MN/m as support stiffness).

Speed [km/h]	**Stress at the imposed limit [MPa]**	**Remaining fatigue threshold [MPa]**								
		R260			**R350HT**			**R400HT**		
		-20° C	*-15° C*	*-10° C*	*-20° C*	*-15° C*	*-10° C*	*-20° C*	*-15° C*	*-10° C*
40	67	56	67	79	174	185	197	216	227	239
80	70	56	67	79	174	185	197	216	227	239
140	74	56	67	79	174	185	197	216	227	239
200	74	56	67	79	174	185	197	216	227	239
300	75	56	67	79	174	185	197	216	227	239

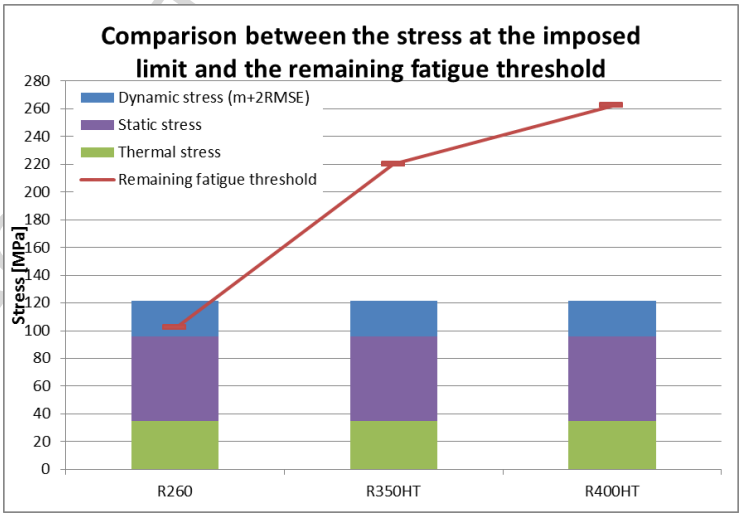

Figure 8: Example of comparison between the stress at the imposed limit and the remaining fatigue threshold at 140 km/h considering three rail steel grades (54E1 rail profile, 30MN/m as support stiffness; -15° C as temperature variation from SFT, 15 tonnes as axle load).

Only in cases of R260 steel grade, which is the most common steel grade in the European railways [17], are there cases which are not verified (i.e. the stress at the imposed limit is higher than the remaining stress capacity), especially at the highest differences from the SFT (-20 and -15° C). In these cases the remaining fatigue threshold is already below the bending stress due to the static load. This can be explained with the fact that a low support stiffness has been used in the simulations to take into account the generally low quality of the ballast close to the irregularity [8]. Possible ways to lower the bending stresses due to the static load include: improving the support stiffness quality [27] or using heavier and stiffer rail section (Figure 9).

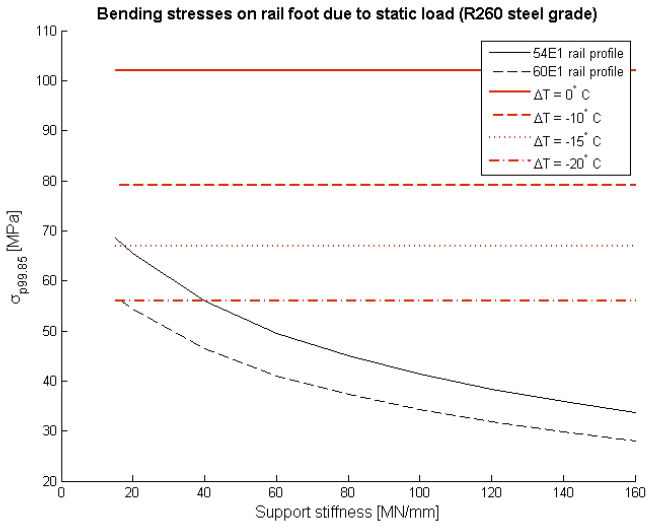

Figure 9: Ways to lower the bending stresses due to the static load in case of R260 steel grade.

As noticed, the support stiffness is influential to the propensity for fatigue failure. Furthermore, the longitudinal weld geometry induces locally increased dynamic forces, which causes increased vibration levels and, thus, an acceleration in the local ballast degradation. This leads to local reduction of support stiffness and further increased dynamic forces (Figure 10) and rail bending stresses. Therefore, it is crucial to maintain a good ballast stiffness (around 80-100 MN/m [21]) near the weld.

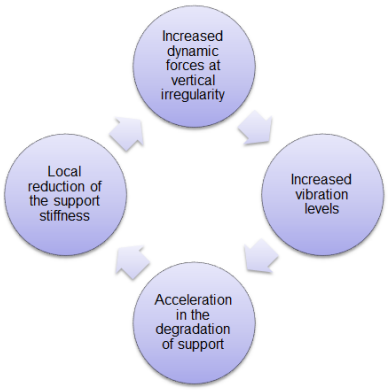

Figure 10: Self-perpetuating relation between dynamic forces and support stiffness.

A general expression that relates the maximum absolute gradient, the support stiffness, the speed and the expected variation from SFT may finally be obtained, by finding the intercept between the variation in bending stresses $\sigma_{s\text{-}d}$ and the remaining stress capacity at the temperature variation ΔT $\sigma_{r\text{-}\Delta T}$.

The total variation in bending stresses $\sigma_{s\text{-}d}$ can be calculated as the sum of rail bending stresses due to static load and dynamic component of the bending stresses:

- *rail bending stresses due to static load*: it is expressed as function of the axle load AL and the support stiffness K_b. It has been calculated using the Beam on Elastic Foundation (BOEF) theory considering 54E1 rail profile and 0.6 m sleeper spacing (Figure 11) [18]:

$$\sigma_s = \frac{0.0684 \cdot AL}{\sqrt[4]{\frac{1200 \cdot 10^6 \cdot K_b}{1200 + K_b}}} \quad (3)$$

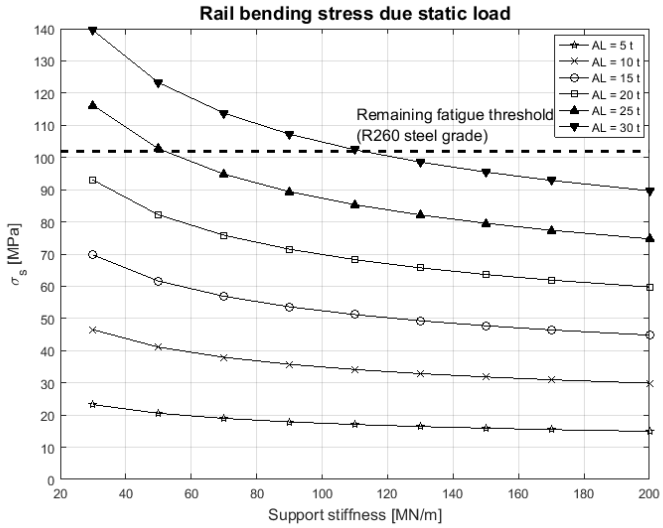

Figure 11: Dependency of the rail bending stresses due to static load on the support stiffness and axle load (54E1 rail profile and 0.6 m sleeper spacing).

- *dynamic component of the bending stresses*: it is expressed as function of weld geometry, support stiffness, speed and unsprung mass:

$$\sigma_d = B(K_b, V, USM) \cdot \tan(\alpha) + 2 \cdot RMSE(K_b, V, USM) \quad (4)$$

The parameter 'B' represents the slope of the regression line in Figure 5 and it is possible to express it through a multivariable regression depending on support stiffness, speed and unsprung mass. Same methodology has been applied to the parameter 'RMSE', which represent the root mean square error associated with each of the line in Figure 5.

The comparison between parameter 'B' (and parameter 'RMSE') from simulation, from a linear regression with speed and a quadratic regression with speed is shown in

Table 11 (and Table 12):

$$\mathrm{RI} = a_1 + a_2 \cdot USM + a_3 \cdot V + a_4 \cdot K_b \tag{5}$$

$$\mathrm{RII} = a_5 + a_6 \cdot USM + a_7 \cdot V + a_8 \cdot K_b + a_9 \cdot V^2 \tag{6}$$

Table 11: Comparison between parameter 'B' from simulation, from a first order regression and a second order regression (in MPa/mrad).

Speed	**40 km/h**			**80 km/h**			**140 km/h**			**200 km/h**			**300 km/h**		
K_b [MN/m]	*SIM*	*RI*	*RII*	*SIM*	*RI*	*RII*	*SIM*	*RI*	*RII*	*SIM*	*RI*	*RII*	*SIM*	*RI*	*RII*
50	2.0	3.1	1.9	4.5	4.5	4.3	7.2	6.6	7.2	9.2	8.8	9.4	11.9	12.3	11.2
70	1.9	3.2	1.9	4.4	4.6	4.3	7.3	6.8	7.3	9.4	9.0	9.5	11.8	12.6	11.4
130	1.9	3.4	1.8	4.4	5.0	4.4	7.9	7.3	7.5	9.5	9.7	9.8	12.1	13.6	12.0
200	1.8	3.7	1.8	4.5	5.4	4.4	7.3	7.9	7.7	10.6	10.4	10.2	12.8	14.5	12.6
Percentage difference with respect to SIM															
50	0%	55%	-5%	0%	0%	-4%	0%	-8%	0%	0%	-4%	2%	0%	3%	-6%
70	0%	68%	0%	0%	5%	-2%	0%	-7%	0%	0%	-4%	1%	0%	7%	-3%
130	0%	79%	-5%	0%	14%	0%	0%	-8%	-5%	0%	2%	3%	0%	12%	-1%
200	0%	106%	0%	0%	20%	-2%	0%	8%	5%	0%	-2%	-4%	0%	13%	-2%

Table 12: Comparison between parameter 'RMSE' from simulation, from a first order regression and a second order regression (in MPa).

Speed	**40 km/h**			**80 km/h**			**140 km/h**			**200 km/h**			**300 km/h**		
K_b [MN/m]	*SIM*	*RI*	*RII*	*SIM*	*RI*	*RII*	*SIM*	*RI*	*RII*	*SIM*	*RI*	*RII*	*SIM*	*RI*	*RII*
50	1.49	2.42	1.91	3.52	2.82	2.86	4.20	3.42	3.91	4.73	4.01	4.51	4.52	5.01	4.51
70	1.45	2.40	1.88	3.54	2.79	2.83	3.72	3.39	3.87	4.56	3.98	4.47	4.50	4.96	4.47
130	1.47	2.31	1.79	3.36	2.69	2.72	3.15	3.25	3.74	3.46	3.82	4.32	4.32	4.77	4.28
200	1.41	2.21	1.69	2.99	2.58	2.61	3.47	3.12	3.61	3.66	3.67	4.16	4.16	4.58	4.09
Percentage difference with respect to SIM															
50	0%	63%	28%	0%	-20%	-19%	0%	-19%	-7%	0%	-15%	-5%	0%	11%	0%
70	0%	66%	30%	0%	-21%	-20%	0%	-9%	4%	0%	-13%	-2%	0%	10%	-1%
130	0%	57%	21%	0%	-20%	-19%	0%	3%	19%	0%	11%	25%	0%	10%	-1%
200	0%	57%	20%	0%	-14%	-13%	0%	-10%	4%	0%	0%	14%	0%	10%	-2%

Table 11 (and Table 12) shows that RI is not reliable enough and that RII gives an acceptable error in the range -6% to +2% (-20% to +30%, especially in case of low speeds) with respect to the SIM model. The quadratic regression with speed is therefore chosen with the following parameters:

$$B = -2.1138 - 0.0026 \cdot K_b + 0.0018 \cdot USM + V \cdot (0.0689 + 0.0004 \cdot K_b - 0.0001 \cdot V) \quad (7)$$

$$RMSE = 0.7630 - 0.0012 \cdot K_b + 0.0001 \cdot USM + V \cdot (0.0325 - 0.0001 \cdot USM - 0.0001 \cdot V) \quad (8)$$

The remaining stress capacity σ_r-$\sigma_{\Delta T}$ at the temperature variation ΔT, instead, can be calculated as the difference of:

- *remaining fatigue threshold*, which is the fatigue stress limit depending on the rail steel grade reduced by the remaining stress. It can be approximated as function of the UTS as in Equation 1;
- *thermal stress* at the variation of the temperature with respect to SFT:

$$\sigma_{\Delta T} = \beta \cdot \Delta T \quad (9)$$

Where:

β = thermal expansion coefficient multiplied by the rail Young's modulus [MPa/ ° C];

ΔT = variation of the temperature with respect to the SFT [° C].

Therefore, the maximum absolute gradient tan(α) which takes into account the rail fatigue life can be expressed as follows (in mrad):

$$\tan(\alpha) = \begin{cases} max\left(\frac{\sigma_r - \beta \cdot \Delta T - \sigma_s(AL,K_b) - 2 \cdot RMSE(USM,V,K_b)}{B(USM,V,K_b)}, 0.7\right), & \sigma_s < \sigma_r - \beta \cdot \Delta T \\ 0.7, & \sigma_s \geq \sigma_r - \beta \cdot \Delta T \end{cases} \quad (10)$$

Where:

σ_r = remaining fatigue threshold [MPa];

β = thermal expansion coefficient multiplied by the rail Young's modulus [MPa/ ° C];

ΔT = variation of the temperature with respect to the SFT [° C];

σ_s = rail bending stress due to static load as in Equation 3 [MPa];

AL = axle load [t];

K_b = support stiffness [MN/m];

RMSE = parameter as in Equation 8 [MPa];

B = parameter as in Equation 7 [MPa/mrad];

USM = half unsprung mass [kg];

V = speed [km/h].

Note that the equation is defined for axle load between 5 and 30 tonnes, speed between 40 and 300 km/h and support stiffness between 50 and 200 MN/m.

The value calculated as in Equation 10 is the optimum and pragmatic maximum absolute gradient if it is not bigger than the current limit imposed by the Dutch Standard at the given speed (Table 13) and if it is not lower than 0.7 mrad which is the pragmatic achievable limit considered with current grinding operation. It is however not excluded and desired that through future development and automation of this process, this value could be reduced.

Table 13: Norm values of the maximum absolute inclination adopted for the QI determination in the Dutch standard (in mrad) [6].

Line speed [km/h]	**Maximum absolute gradient (25 mm basis)**
40	3.2
80	2.4
140	1.8
200	1.3
300	1.0

Table 14 summarises the proposed limits (shown in red) applying Equation 10 considering three axle loads (10/15/25 tonnes equivalent to low/medium/high axle load), three types of track bed and three types of temperature changes (-30° /-15° /-10° from the SFT). In the cases in which the limits calculated by the Dutch Standards indicate a tighter control, the limits for these cases have been replaced by those from the Dutch Standard (shown in black). Note that the proposed values refer to a 54E1 rail section and R260 steel grades.

Table 14: Proposed gradient limits for three axle loads, three types of track bed and three average changes in temperature from SFT (values in mrad – R260 steel grade, 54E1 rail section).

Speed [km/h]	Track bed type	Up to 10 t			Up to 15 t			Up to 25 t		
		Down to -30° C	*Down to -15° C*	*Down to -10° C*	*Down to 30° C*	*Down to -15° C*	*Down to -10° C*	*Down to -30° C*	*Down to -15° C*	*Down to -10° C*
40	Soft	2.4	3.2	3.2	0.7	0.7	3.2	0.7	0.7	0.7
	Typical	3.2	3.2	3.2	0.7	1.8	3.2	0.7	0.7	0.7
	Stiff	3.2	3.2	3.2	3.2	3.2	3.2	0.7	0.7	3.2
80	Soft	1.2	2.4	2.4	0.7	0.7	1.9	0.7	0.7	0.7
	Typical	1.8	2.4	2.4	0.7	0.7	2.4	0.7	0.7	0.7
	Stiff	2.4	2.4	2.4	1.0	2.4	2.4	0.7	0.7	2.3
140	Soft	0.7	1.8	1.8	0.7	0.7	0.7	0.7	0.7	0.7
	Typical	1.1	1.8	1.8	0.7	0.7	1.4	0.7	0.7	0.7
	Stiff	1.8	1.8	1.8	0.7	1.8	1.8	0.7	0.7	0.9
200	Soft	0.7	1.3	1.3	0.7	0.7	0.7	0.7	0.7	0.7
	Typical	0.8	1.3	1.3	0.7	0.7	0.9	0.7	0.7	0.7
	Stiff	1.3	1.3	1.3	0.7	1.1	1.3	0.7	0.7	0.7
300	Soft	0.7	1.0	1.0	0.7	0.7	0.7	0.7	0.7	0.7
	Typical	0.7	1.0	1.0	0.7	0.7	0.7	0.7	0.7	0.7
	Stiff	1.0	1.0	1.0	0.7	0.7	1.0	0.7	0.7	0.7

5. Conclusions and recommendations

A series of parametric simulations have been undertaken to investigate the influence of the longitudinal geometry of weld profiles on the propensity for rail and track degradation. The work builds on the existing relationship between longitudinal gradient and wheel-rail contact force derived by Steenbergen [7, 10].

The study here extended the existing work to include a wider range of input parameters, including track parameters (e.g. support stiffness, sleeper type and spacing, rail type) and vehicle parameters (e.g. speed, USM and primary suspension characteristics), and consider a broad range of rail and track damage metrics, including contact forces, bending stresses and ballast forces.

From a parametric study, which utilised theoretical and measured longitudinal weld profiles it was concluded that:

- Supporting the findings of Steenbergen [2, 7-10], the maximum absolute gradient of the longitudinal weld profile is a suitable proxy for wheel-rail contact force in the context of a standard;
    - The maximum permissible gradient tan(α) is inversely proportional to the speed V, for a given maximum acceptable dynamic force $F_{dyn,max}$:

$$\tan(\alpha) = \frac{F_{dyn,max}}{0.20 \cdot V} \tag{11}$$

    - This relation indicates that, for a given maximum allowable dynamic force, a tighter control of geometry is required for higher speed lines;

    - The limits proposed in the Dutch standard (see Table 13) have been further investigated in this project by considering the wheel/rail contact forces. They aim to be optimum and yet pragmatic limits, in terms of maintenance capabilities, in order to achieve good weld geometries but the aspiration to achieve improved weld geometry through improved and ideally automated process, i.e. to achieve consistency of quality, still remains.

- A combination of low track support stiffness and light rail section can lead to higher susceptibility to rail foot fatigue when associated with higher tensile stresses, such as those associated with ambient temperatures significantly below the SFT (10° C below or greater). In these conditions the risk of rail break can be reduced by:
    - improving weld geometry;
    - improving track support quality;
    - increasing rail section size (i.e. second moment of area).
- Further investigations, considering not only the contact forces but also the total bending stresses imposed and the rail fatigue life, have led to recommended tighter controls for the longitudinal profile depending on steel grade, support type, the USM, the axle load, the speed and variation with respect to the SFT (Equation 10)
- The correlation and dependency between the maximum absolute gradient and the wheel-rail force and maximum rail bending stress was also found to increase with increasing axle load;
    - Consequently, tighter geometric controls may be required on routes with high axle load traffic (e.g. freight routes), especially because, under these conditions, wear and plastic deformation of the weld area will lead to accelerated amplification of dynamic load and subsequent degradation.

Based on the findings presented in this paper the following recommendations are made.

- First-derivative based methods should be used for the assessment of the quality of the weld geometry, instead of the current zero-derivative methods.

- The limits for the optimum profile should be based on the maximum total bending stresses imposed and the rail fatigue life, as well as wheel-rail contact forces.

Acknowledgement

The present work has been undertaken within the European Project WRIST (Grant agreement 636164), part of the Horizon 2020 program.

References

1. Ishida, M., et al., *Influence of Loose Sleeper on Track Dynamics and Bending Fatigue of Rail Welds.* Quarterly report of RTRI, 1999. **40**(2): p. 80-85.
2. Steenbergen, M.J.M.M. and R.W. van Bezooijen, *Rail welds*, in *Wheel-rail interface handbook*, R. Lewis and U. Olofsson, Editors. 2009, Woodhead Publishing Limited: Cambridge.
3. WRIST, *Deliverable D1.4: Parametric studies to inform the optimum and pragmatic weld profile (Confidential)*. 2016.
4. European Committee For Standardization, *EN 14730-2 Railway applications - Track - Aluminothermic welding of rails - Part 2: Qualification of aluminothermic welders, approval of contractors and acceptance of weld*. 2006: Brussels.
5. European Committee For Standardization, *EN 14587-1 Railway applications - Infrastructure - Flash butt welding of rails - Part 1: New R220, R260, R260Mn, R320Cr, R350HT, R370LHT and R400HT grade rails in a fixed plant*. 2016: Brussels.
6. ProRail, *Directives RLN00127 - Part 1 & Part 2*. 2007: Utrech.
7. Steenbergen, M.J.M.M. and C. Esveld, *Rail weld geometry and assessment concepts.* Proceedings of the Institution of Mechanical Engineers, Part F: Journal of Rail and Rapid Transit, 2006. **220**(3): p. 257-271.
8. Steenbergen, M.J.M.M. and C. Esveld, *Relation between the geometry of rail welds and the dynamic wheel-rail response: numerical simulations for measured welds.* Proceedings of the Institution of Mechanical Engineers, Part F: Journal of Rail and Rapid Transit, 2006. **220**(4): p. 409-423.
9. Steenbergen, M.J.M.M., *Quantification of dynamic wheel–rail contact forces at short rail irregularities and application to measured rail welds.* Journal of Sound and Vibration, 2008. **312**(4): p. 606-629.
10. Steenbergen, M.J.M.M., *Modelling of wheels and rail discontinuities in dynamic wheel–rail contact analysis.* Vehicle System Dynamics, 2006. **44**(10): p. 763-787.
11. Gao, J., W. Zhai, and Y. Guo, *Wheel–rail dynamic interaction due to rail weld irregularity in high-speed railways.* Proceedings of the Institution of Mechanical Engineers, Part F: Journal of Rail and Rapid Transit. **0**(0): p. 0954409716664933.
12. Mutton, P.J. and E.F. Alvarez, *Failure modes in aluminothermic rail welds under high axle load conditions.* Engineering Failure Analysis, 2004. **11**(2): p. 151-166.
13. Grossoni, I., et al., *Dynamics of a vehicle–track coupling system at a rail joint.* Proceedings of the Institution of Mechanical Engineers, Part F: Journal of Rail and Rapid Transit, 2015. **229**(4): p. 364-374.
14. RailProf Instruments BV, *RAILPROF user manual*. 2010.
15. Jenkins, H., et al., *The effect of track and vehicle parameters on wheel/rail vertical dynamic forces.* Railway Engineering Journal, 1974. **3**(1): p. 2-16.
16. Hunt, G.A., *EUROBALT: vertical dynamic model for track damage studies*. 1996, British Rail Research.
17. WRIST, *Deliverable D1.1: Selection of rail section and grade (Confidential)*. 2015.

18. Esveld, C., *Modern railway track*. Vol. 385. 2001: MRT-productions Zaltbommel, The Netherlands.

19. Remington, P.J., *Wheel/rail rolling noise, I: Theoretical analysis.* The journal of the Acoustical Society of America, 1987. **81**(6): p. 1805-1823.

20. Steenbergen, M. and C. Esveld, *Rail weld geometry and assessment concepts.* Proceedings of the Institution of Mechanical Engineers, Part F: Journal of Rail and Rapid Transit, 2006. **220**(3): p. 257-271.

21. Terashita, Y. and M. Tatsumi, *Analysis of damaged rail weld.* Quarterly Report of RTRI, 2003. **44**(2): p. 59-64.

22. Whitney, B., *The importance of track formation stiffness*. 2015, Permanent Way Institution.

23. Murray, M.H. *Rail fatigue and the role of impact forces*. in *Proceedings of the 11th International Heavy Haul Conference*. 2015. International Heavy Haul Association (IHHA) Inc.

24. Archard, J.F., *Contact and Rubbing of Flat Surfaces.* Journal of Applied Physics, 1953. **24**(8): p. 981-988.

25. European Committee for Standardization, *EN13674 - 1 Railway Applications. Track. Rail. Part 1: Vignole railway rails 46kg/m and above*. 2011.

26. Zerbst, U., et al., *Introduction to the damage tolerance behaviour of railway rails - a review.* Engineering Fracture Mechanics, 2009. **76**: p. 2563-2601.

27. Cross Industry Track Stiffness Working Group, *A guide to track stiffness*. 2016: Southampton.

Longitudinal rail weld geometry control and assessment criteria

Ilaria Grossoni, Philip Shackleton, Yann Bezin, Jay Jaiswal

Highlights

- The first-derivative assessment method is confirmed suitable in context of standard
- Light rail section on low track quality may be susceptible to rail foot fatigue
- Tighter weld geometry controls based on total bending stresses are proposed